Low Temperature Physics/Fizika Nizkikh Temperatur, 2021, vol. 47, No. 9, pp. 804–818

Dynamics, properties and spectrum of reconnecting vortex loops in superfluid helium

(Review Article)

L. P. Kondaurova[1,2] and V. A. Andryushchenko[1,3]

[1]*Kutateladze Institute of Thermophysics, Siberian Branch of the RAS, Novosibirsk 630090, Russia*

[2]*National Research University "Moscow Power Engineering Institute", Moscow 111250, Russia*

[3]*Novosibirsk State University, Novosibirsk 630090, Russia*

E-mail: louisa@ngs.ru; vladimir.andryushchenko@gmail.com

Received April 05, 2021, published online July 26, 2021

The quantum turbulence is a collection of the interacting quantum vortex loops and filaments. The main goal of this work is to systematize the information on the current state of the research on the reconnecting quantized vortex loops in the superfluid helium: the geometry, the dynamics, the properties of the vortex loops, the energy spectrum before and after the reconnections. The paper discusses the possible role of the reconnections in the formation of the turbulent spectrum. In addition, in this paper the main methods and approaches to the study of the reconnecting vortex loops and quantum turbulence are discussed.

Keywords: superfluid helium, vortex loops, reconnections, energy spectrum.

Contents

1. Introduction

If the helium isotope ^{4}He is cooled to a temperature of $T_\lambda \approx 2.17$ K, it undergoes a phase transition and becomes a quantum liquid. One of the manifestations of the quantum properties of a liquid is the phenomenon of superfluidity, i.e., the ability of the helium to flow without friction. Firstly the superfluidity was discovered in ^{4}He. In this temperature range, helium has a number of unique properties that are associated with the quantum nature of this liquid. This phase state is usually denoted as He II. The mechanism for the onset of the superfluidity was explained by means of the Bose–Einstein condensation. The spin of the helium atom is zero. Therefore the helium atoms are the bosons, and the ensemble of the helium atoms obeys the Bose–Einstein statistics.

An ideal gas of the bosons consist of particles with non-zero rest mass. It can pass into the state of a Bose–Einstein condensate. At low temperatures, the particles tend to occupy a lowest energy level, forming a condensate. A similar effect is observed in a liquid helium. The formation of condensate associated with the superfluid component begins

at a temperature below the λ point. The ground state of He II is a completely superfluid liquid. The idea that the superfluid component is a single coherent quantum state was formulated by London (1938, 1954) [1–3]. Therefore its properties can be described by introducing a macroscopic wave function.

The physical model of the hydrodynamics of a superfluid helium was built by Tisza (1938, 1947) [4, 5] and Landau (1941–1949) [6–9]. The essence of this model is the coexistance of two movements (the normal and superfluid movements) in the superfluid helium. Each of these movements is associated with its own effective density ρ_n and ρ_s, respectively. Then the density of the liquid helium ρ is determined by the following expression $\rho = \rho_n + \rho_s$. The superfluid movement is a potential movement, it does not transfer entropy, there is no shear viscosity, and the chemical potential gradient is a driving force. The normal movement corresponds to the movement of a classical fluid. This is the other significant difference between a superfluid liquid and a classical liquid. At a temperature of about 1 K, the normal movement practically stops, and the portion of the normal component becomes less than one percent [10]. At these temperatures there is practically no energy dissipation.

Another manifestation of the quantum properties of the He II is the presence of the quantum vortices in the superfluid component of a helium [11]. Various methods of influencing the liquid can lead to the development of the vortices [12–16]. A distinctive feature of these vortices from the vortices in a classical fluid is that the circulation of the velocity of the superfluid component is quantized: $\oint_C \mathbf{v}_s \cdot d\mathbf{l} = n\kappa$. The integration goes along a closed curve C (a curve without self-intersections) in a superfluid, $\kappa = h / m_{\mathrm{He}_4}$ is the quantum of the velocity circulation, h is the Planck's constant, m_{He_4} is the mass of a helium atom, n is an integer. The diameter d of the core of these vortices is approximately the several interatomic distance $d \approx 10^{-8}$ cm. The vortex tangle consisting of these vortex lines is called the superfluid turbulence.

A special interaction arises between the normal and superfluid movements, which is called the force of mutual friction. As a result, an additional energy dissipation arises, which is not in a classical liquid. The role of the quantum vortices is significant. They, in fact, determine the hydrodynamic and thermodynamic properties of He II. Today, an active study of the dynamics and properties of these vortices is continued [17–31]. A certain interest in them comes out beyond the region of the superfluid helium. For example, the idea that classical turbulence can be modeled by a set of thin vortex tubes is being actively discussed. In the paper [32] it is discussed the current state of this approach.

The superfluidity also occurs in the many other systems: in the liquid of the isotope ^{3}He at the temperatures below $T_c \approx 10^{-3}$ K at a saturated vapor pressure [33], in the Bose–Einstein condensates [34–37], in the system of ultracold atoms [38], in the exciton-polariton superfluids [39–41], in the quantum liquids of light [42], in the system of the Bose–Einstein quasi-equilibrium magnons (the spin superfluidity) [43, 44] and etc. Ones demonstrate all the diversity of the superfluid behavior: the frictionless flow, the vortices, etc. For many years, quantum liquids were studied both experimentally and theoretically. Nowadays, it has become one of the main directions in the physics of low temperatures. The applications of the superfluidity phenomena are very diverse, one can see the work [22] and the references therein.

The aim of this work is to present the current state of the art in the study of geometry, the dynamics, the properties of the vortex loops and the energy spectrum of the reconnecting quantized vortex loops in the superfluid helium. Recently, new methods have been developed for a visualization of the vortex filaments in the superfluid ^{4}He [22, 45–47]. The development of these methods and their application is the great importance for the studying of the properties of vortex structures. As a result, significant progress in the understanding of quantum turbulence is possible in the near future. In addition, the real opportunity appears to compare the theoretical results with the experiments.

2. Methods and approaches to study the quantum turbulence

The articles devoted to the numerical modeling of the vortex tangle dynamics can be divided into the studies using the Gross–Pitaevskii equation [48], into studies using the vortex line method [49, 50], and into studies carried out within the framework of the equations of the hydrodynamics of the superfluid turbulence. Before proceeding with the analysis of the results of these works, let us recall the methods and approaches.

2.1. Gross–Pitaevskii equation

The Bose–Einstein condensate is a very useful model to study the dynamics of the vortices in quantum fluids near the absolute zero (in the absence of mutual friction in the ^{3}He and ^{4}He fluids). However, some results should be used with caution. The point is that the Gross–Pitaevskii equation (the nonlinear Schrödinger equation) describes a weakly interacting Bose gas:

$$i\hbar \frac{\partial \Psi(r,t)}{\partial t} = \left(-\frac{\hbar^2}{2m}\nabla^2 + V_{\mathrm{ext}} + g\,|\,\Psi(r,t)\,|^2 - \mu \right)\Psi(r,t). \tag{1}$$

Here $\Psi(r,t)$ is the condensate's complex wave function (the order parameter), g is the strength of the interaction between the bosons, μ is the chemical potential, and m is the boson mass, V_{ext} is the potential of the field in which the bosons move, r is a coordinate, t is a time. The condensate's density $\tilde{\rho}_s$ and the velocity u_s are related to $\Psi = |\,\Psi\,| e^{(i\Theta)}$ via Madelung transform: $\tilde{\rho}_s = m\,|\,\Psi\,|^2$, $u_s = \hbar\nabla\theta / m$. It can

be shown that on the length scales R when $R \gg \xi = \hbar/\sqrt{2m\mu}$ (ξ is the "internal" length parameter, is the correlation radius [51]), the Gross–Pitaevskii equation is reduced to of the modified classical Euler equations for a compressible medium.

Unlike a weakly interacting gas, the superfluid helium is a liquid, and interaction forces between its molecules are much greater then the interaction forces between bosons. In addition, only part of the superfluid component is condensed. Moreover, the parameters used in numerical studies based on the Gross–Pitaevskii equation lead to the following value of the ratio of the vortex core radius a_0 to the intervortex distance ξ ($a_0/\xi \sim 0.1$–0.3) which is not extremely small. In the superfluid helium this ratio lies in the range 10^{-5}–10^{-8}. Therefore the velocity of the moving of the filament elements in the condensate is not too low compared to the speed of sound. Indeed, the value of the speed of sound c is of the order of κ/a_0, the velocity of the filament elements is $v_l \sim \kappa/\delta$. Therefore, the Mach number $M = v_l/c \sim a_0/\delta$ is not an extremely small value. The intensity of the sound emission is related to the Mach number M. Thus, a large-scale movement of the filament (such as long Kelvin waves) emits a sound. In quantum liquids, this process takes place only for the extremely short waves. Despite the differences described above, the solutions of the Gross–Pitaevskii equation provide useful information about the dynamics of the vortex filaments.

At the high temperatures, the damping potential (an analog of the mutual friction force) [52, 53] is introduced into the Gross–Pitaevskii equation.

2.2. Vortex filament method

This method was suggested by Schwarz [49, 50]. Schwarz made the assumption that the densities of the normal and superfluid components remain constant when the temperature of the liquid does not change. This means that all physical phenomena associated with the compressibility of a liquid, in principle, cannot be investigated in this approach. This is an additional difference between the studies based on the Gross–Pitaevskii equation and studies that use the vortex line method. Assuming that the diameters of the cores of the quantized vortices do not change, and the vortices themselves are the infinitely thin filaments, the velocity for the points of the vortex filament was found in the works [49, 50]:

$$\mathbf{V}_B = \beta \mathbf{s}(\xi) \times \mathbf{s}''(\xi) + \frac{\kappa}{4\pi} \int_C \frac{(\mathbf{s}(\xi') - \mathbf{s}(\xi)) \times \mathbf{s}'(\xi')}{|\mathbf{s}(\xi') - \mathbf{s}(\xi)|^3} d\xi',$$

$$\beta = \frac{\kappa}{4\pi} \ln\left[\frac{2\sqrt{l_+ l_-}}{e^{1/4} a_0}\right], \qquad (2)$$

where the parameter ξ is the length of a filament segment. The integral accounts for the influence of the whole vortex configuration C, excluding the segments adjacent to $\mathbf{s}(\xi)$. The prime in $\mathbf{s}'$ denotes the derivative with respect to the instantaneous arc length ξ, e.g., $\mathbf{s}' = d\mathbf{s}/d\xi$. $\mathbf{s}'' = d^2\mathbf{s}/d\xi^2$ is the second derivatives by parameter ξ. Here, $l_\pm$ are the lengths of elements length adjacent to $\mathbf{s}(\xi)$, $e = 2.71\ldots$ is the base of the natural logarithm. The Biot–Savart integral (2) diverges at the points where $\mathbf{s}(\xi', t) = \mathbf{s}(\xi, t)$. To avoid this divergence, a cutoff parameter was introduced. The cutoff value is approximately equal to the core radius value [54–57]. The velocity of moving of the points of the vortex line $\mathbf{V}_L$ is the sum of the velocity of moving of the superfluid component of the fluid $\mathbf{V}_s$ and the velocity $\mathbf{V}_B$ induced by all vortex filaments. When the quantized vortices appear, they interact with the normal component (the mutual friction force), which leads to a change in the velocity of the vortex filament. Thus, the expression for determining the velocity of the points of the vortex line takes the following form:

$$\mathbf{V}_L = \mathbf{V}_s + \mathbf{V}_B + \alpha \mathbf{s}' \times (\mathbf{V}_{ns} - \mathbf{V}_B) - \alpha' \mathbf{s}' \times [\mathbf{s}' \times (\mathbf{V}_{ns} - \mathbf{V}_B)], \qquad (3)$$

where α and α' are the temperature-dependent friction coefficients, $\mathbf{V}_{ns} = \mathbf{V}_n - \mathbf{V}_s$ is the counterflow velocity, $\mathbf{V}_n$ is the velocity of the normal component of helium. To find the velocity of the elements of the vortex filaments, it is necessary to determine the value of the induced velocity $\mathbf{V}_B$. To find this velocity for each element of the filaments, it is necessary to determine the contribution from the entire configuration of the filaments, and this requires rather large computational load. Therefore, the so-called local approximation is often used in the calculations, when the movement of the vortex thread point is determined only by the adjacent segments of the vortex filaments:

$$\mathbf{V}_{si} = \beta_{\text{loc}} \mathbf{s}' \times \mathbf{s}'', \qquad \beta_{\text{loc}} = c\kappa/4\pi \ln(R/a_0). \qquad (4)$$

Aarts [57] showed that the best approximation of the velocity of the vortex points [see Eq. (4)] is achieved when the constant $c = 1.1$. There is another important contribution to the velocity of vortex filaments, which is associated with the processes of reconnection of filaments. As a result of the reconnections, the topology of the vortex structure changes. Merging of two vortex loops forms a new larger loop. When the loops are broken, the smaller loops are formed. In both cases, the disturbances arise along the vortex filaments, so-called Kelvin waves. The processes of reconnection of vortex loops are not described analytically. In the numerical works, starting with the work of Schwartz, the various reconnection criteria are used [58–64]. These criteria base on physical intuition and numerical simulation results. The influence of reconnection processes on the properties of a vortex tangle (a set of vortex filaments) is studied in the work [19] in detail. In addition, the influence of various criteria for the realization of the reconnections on the properties and dynamics of a vortex is investigated in this work.

2.3. Hydrodynamics of superfluid turbulence

The superfluid helium model proposed by Tisza [4, 5], Tisza and Landau [6–8] describes the hydrodynamics of the superfluid helium when the quantized vortices are absent. The effect of the quantum vortex filaments is taken into account by introducing the Gorter–Mellink force [11] into the right part of the Landau–Khalatnikov equations in the following form: $\mathbf{F}_{sn} = A(t)\rho_s\rho_n\mathbf{V}_{ns}^3$ (although this approach is incorrect). Here $A(t)$ is the temperature depended constant of Gorter–Mellin. Further improvement was in the representation of this force in the following form: $\mathbf{F}_{sn} = A(t)\rho_s\rho_n\mathcal{L}\mathbf{v}_{ns}$. Here $\mathcal{L}$ is the density of vortex lines per unit volume. With this approach, the dynamics of the quantity $\mathcal{L}$ is assumed to be described by the Vinen equation [65–68]:

$$\frac{d\mathcal{L}}{dt} = \alpha\,|\,\mathbf{V}_{ns}\,|\,\mathcal{L}^{3/2} - \beta\mathcal{L}^2. \qquad (5)$$

Here α, β are the coefficients that depend on the temperature. However, this approach also has a limited applicability.

Further, attempts to construct the hydrodynamics of He II led to the various variants of their production: the phenomenological approach [69], the stochastic approach [70], the variational approach [71]. In essence, these equations are the Landau–Khalatnikov equations, into which the Vinen equation is incorporated. Note that the structure of vortex lines is disordered in this case. These equations allowed us to describe many of the phenomena observed in experiments, see, for example, [72–75].

Let us consider an alternative approach for obtaining a system of hydrodynamic equations in the presence of vortex quantized lines in He II. It is assumed that bundles of unidirectional lines are formed in the volume of the liquid (for example, when the liquid flows around any obstacles, or there is the counterflow) as in the case of rotation of a liquid in a container. It is assumed that in this way the superfluid motion adapts to the normal motion. Further, it is assumed that $\mathcal{L} = \omega/\kappa$ ($\boldsymbol{\omega} = \mathrm{rot}\,\mathbf{V}_s$ is the vorticity). As a result, a system of hydrodynamic equations for the He II was obtained [76–78] basing on the Hall–Vainen–Bekarevich–Khalatnikov model for a rotating fluid:

$$\rho_s\left[\frac{\partial\mathbf{V}_s}{\partial t} + (\mathbf{V}_s\cdot\nabla)\mathbf{V}_s\right] = -\nabla p_s - \rho_s\mathbf{f}_{ns},$$

$$\rho_n\left[\frac{\partial\mathbf{V}_n}{\partial t} + (\mathbf{V}_n\cdot\nabla)\mathbf{V}_n\right] = -\nabla p_n + \mu\nabla^2\mathbf{V}_n + \rho_s\mathbf{f}_{ns},$$

$$\mathbf{f}_{ns} = \alpha\hat{\boldsymbol{\omega}}_s\times(\boldsymbol{\omega}_s\times\mathbf{V}_{ns}) + \alpha'\hat{\boldsymbol{\omega}}_s\times\mathbf{V}_{ns}. \qquad (6)$$

Using these equations (for example, in [78–81]), the semiclassical behavior of the quantum turbulence is shown. The problems associated with the application of these approaches are discussed in the works [82, 83].

The processes directly related to the reconnection of vortex loops can be conditionally divided into the three main stages: the convergence of the elements of the vortex loops, the actual realization of the reconnection, and the relaxation of the disturbances arising during reconnection. Note that, despite the large number of the works devoted to the dynamics of reconnecting vortex loops, the exact theory of this process has not yet been built. Thus, all the existing results were obtained in the experiments, or using numerical simulation or semi-empirical models.

2.4. Evolution of the vortex loops before the reconnection

Let us consider in more detail the first stage of reconnection — the stage of convergence of the elements of the vortex loops. Due to the interaction between the vortex loops, they can approach to each other. The pyramid-like protrusions appear on the approaching elements of the vortex loops, see Fig. 1 [84]. Such protrusions are called kinks.

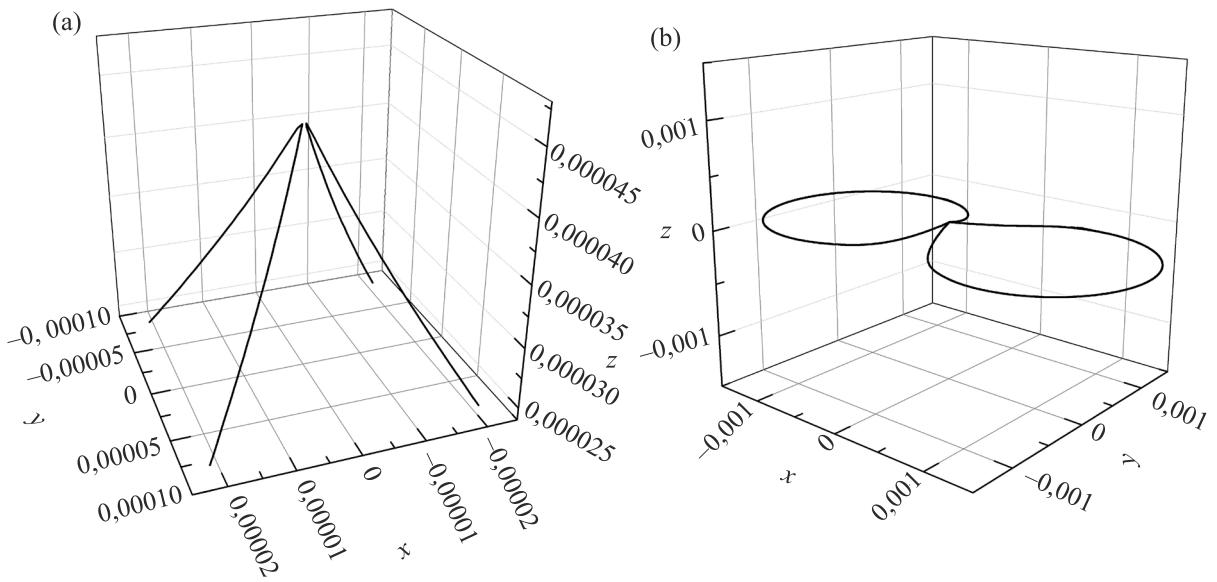

Fig. 1. Geometric configuration of kinks (a) and vortex loops (b) before reconnection. The linear dimensions are measured in centimeters.

As the vortex loops approach, the kinks begin to grow. The curvature at their nearest points (the tops of the kinks) also increases. An increase in curvature leads to an increase in the induced velocity of the nearest vortex loop elements [see Eq. (4)] and, accordingly, to an acceleration of their convergence. For the mathematical description of this process, two characteristics are usually used: the dependence of the minimum distance between the elements of the vortex loops on time $\delta(t)$ and the geometric parameters of the kinks. The first characteristic is of particular interest since it is closely related to the rate of reconnections (the number of reconnections per unit time). In turn, the second characteristic plays a decisive role in the formation of a three-dimensional velocity field induced by the reconnecting vortices.

For the first time, Schwarz [49, 50] pointed out the necessity to take into account the vortex loop reconnections when calculating quantum turbulence. In these works, he also proposed a vortex filament model, which is subsequently actively used in the numerical study of the reconnections.

2.4.1. Time dependence of the minimum distance between the elements of the vortex loops

Developing Schwartz ideas, Koplik and Levine [85] perform the first numerical simulation of the quantum vortex reconnections solving the Gross–Pitaevskii equation (1). As a result, it was found that the vortex filaments should reconnect when approaching to each other at a distance of the order of several radii of the vortex filament core.

A little later, De Waele and Aarts [86] investigate the dynamics of the vortex filaments before the reconnection at zero temperature using the vortex filament method in the local approximation of the Biot–Savart equation (4). Their calculations show that the time dependence of the distance between the nearest elements of the vortex loops does not depend on the initial conditions and has an universal form:

$$\delta(t) = \sqrt{(\kappa / 2\pi)(t_* - t)}, \tag{7}$$

here t_* is the reconnection time, (the interval between the initial moment of the modeling and the moment of reconnection). For the first time experimentally the reconnections in He II are studied in the temperature range from 1.7 to 2.05 K by Paoletti *et al*. [87]. In this work, solid hydrogen particles are used as tracers to visualization the motion of the vortex filaments. The obtained data (before and after the connections) for all temperatures are described by the dependence:

$$\delta(t) = A\sqrt{\kappa\,|\,t_* - t\,|}(1 - c\,|\,t_* - t\,|), \tag{8}$$

here $A \approx 1.25$ and $c \approx 0.5\ \mathrm{s}^{-1}$. It should be noted that the standard deviation of the obtained coefficients A and c is large enough in comparison with their average value to finally draw a conclusion about the nature of the studied dependence.

After the experiment, a series of numerical works appeare which are performed both within the frame of the Gross–Pitaevskii equation [88–93] and within the vortex filament method [89–98]. Next, we consider the main results obtained in them.

Information on the convergence of the elements of the vortex filament before reconnection was obtained in the work of Tsubota [95] based on the vortex filament method and the complete Biot–Savart equation (2). So the data is well described by the Eq. (8). However, the obtained coefficient $A \approx 3$ significantly exceeds the experimental values obtained in [87].

Tebbs *et al*. [88] confirm the root law of the convergence of the vortex loop elements by numerically solving the Gross–Pitaevskii equation, but their data are better described by the Eq. (8) with different values of the coefficients for the different conditions.

Kursa *et al*. [89] perform the numerical simulations of the reconnections of the quantum vortex loops, solving both the Gross–Pitaevskii equation and the Biot–Savart equation. As was found in their work the reconnection of two almost antiparallel vortices can lead to the creation of a cascade of vortex rings in the condition of the enough small angle between the planes of the vortices. Thus, a significant dependence of reconnections on the initial conditions is demonstrated. It should be noted that, unlike the reconnections in superfluids, the exponents in equations like (7), (8) for the classical fluids before and after reconnection are different [99].

Zuccher *et al*. [90] simulated the reconnections using the Gross–Pitaevskii and Biot–Savart models at zero temperature. The dynamics of vortices before and after reconnection are studied for the different angles β between the planes of their initial location. The obtained results (for the Gross–Pitaevskii model) are described by the equation:

$$\delta(t) = A\,|\,t_* - t\,|^{\alpha}\,. \tag{9}$$

On average, before a reconnection $\alpha^-_{\mathrm{ave}} \approx 0.39$ and $A^-_{\mathrm{ave}} \approx 1.39$, after a reconnection $\alpha^+_{\mathrm{ave}} \approx 0.68$ and $A^+_{\mathrm{ave}} \approx 1.54$. When the angle value $\beta = \pi$: $\alpha^- \approx 0.3$ and $A^- \approx 1.36$; $\alpha^+ \approx 0.66$ and $A^+ \approx 1.88$. If the value is $\beta = \pi/2$: $\alpha^- \approx 0.36$ and $A^- \approx 1.41$, $\alpha^+ \approx 0.67$ and $A^+ \approx 1.01$. Here the exponents before and after a reconnection are different, as in the classic fluids [99]. In addition, it is shown in [90] that small rings appear at the time of reconnection, as in [89]. Moreover, at that time the Kelvin waves appear also. In the case of the Biot–Savart equation, only the values of the angle $\beta = \pi$ and $\beta = \pi/2$ are studied. The root dependence $\delta(t)$ is preserved, however, after reconnection of the vortices, the obtained results are described by the dependence:

$$\delta(t) = \sqrt{\kappa \cdot \pi\,|\,t_* - t\,|}, \tag{10}$$

thus the divergence of the nearest elements of the vortex loops occurs at a higher speed than their convergence before the reconnection.

Using the vortex filament method, Hanninen [94] investigated the dynamics of the vortex filaments before and after the reconnection at different temperatures.

The resulting relationship is described by Eq. (9), with $\alpha = 1/2$ and $A^- = \sqrt{\kappa/16}$, $A^+ = \sqrt{8\cdot\kappa}$, that slightly differs from the coefficients obtained in [90] [see Eq. (10)].

Also, numerical studies of the dynamics of the vortex filaments are carried out in the works [91–93]. The Gross–Pitaevskii equation is chosen in them as basic model.

Allen *et al*. [91] obtained at all temperatures the values of δ that are described by Eq. (9): $\alpha^- = 0.41 \pm 0.02$, $\alpha^+ = 0.66 \pm 0.02$ and $A^\mp = \kappa$. As in the work [90], different exponents are obtained here before and after reconnection of the vortex lines.

For the initial value of the angle $\beta = \pi$ between the planes of the vortex loops Rorai *et al*. [92] obtained the relation $\delta^\mp \sim |t_* - t|^{1/2}$, for $\beta = \pi/2$: $\delta^- \sim (t_* - t)^{1/3}$, $\delta^+ \sim (t_* - t)^{2/3}$.

In the work of Villois and Proment [93], an independent of the initial configuration of the vortex loops relation was obtained: $\delta^\mp \sim (t_* - t)^{1/2}$, but the coefficient $A^\mp$ depends on the initial configuration of the vortex loops.

The dynamics of vortex filaments before and after the realization of the reconnection at the different temperatures and initial conditions is also studied in the frame of the vortex filament method using the full Biot–Savart equation in a series of works [96–98]. As a result of systematic modeling, the time dependences of the minimum distance between the elements of the vortex loops are obtained for the various temperatures and initial configurations. Additionally, during simulation of the dynamics of the quantized vortices before the reconnections, the nature of their convergence is established. In particular, three characteristic stages in the evolution of the vortices before the reconnections were identified, and the boundaries between them were established. In each of the stages, the dynamics of the nearest elements of quantized vortices is conditioned by the ratio of the forces of intervortex interaction and the forces of interaction between the vortices and the normal component of helium. It is found that only the dynamics of the vortex filaments immediately before the reconnection (starting from the distances $0.07 - 0.08R_0$ from the reconnection point, where R_0 is the initial radius of the vortex ring) has a universal character, independent of the temperature and the initial location of the vortex filaments. Only on these scales the velocity of the nearest elements of the vortex loops is well described by Eq. (7). At the larger distances from the reconnection point, the friction has a more significant effect on the dynamics of the vortex loops. In this case, the dynamics of the elements of the vortex loops is described by an equation of the type (8), which agrees with the experimental data [87]. Farther away from the reconnection point, the dynamics of the vortex loops is generally not universal. Right up to the situation when at the high temperatures the vortex loops can collapse (decrease in size, turning into thermal excitations or emitting a second sound) even before the reconnection occures.

Thus, for the approaching vortex loops, the several time dependences of the minimum distance between the elements of the vortex loops are obtained. For the dependences obtained by the vortex filament method, the differences are only quantitative, i.e., $\delta(t) \sim (t_* - t)^{1/2}$ both before and after reconnection. This circumstance can be associated with the choice of the time interval for the approximation of $\delta(t)$, since for points far from the reconnection point, the dependence $\delta(t)$ is influenced by the initial conditions [97]. It is important to note that the initial conditions in all of the listed works were different. For the dependences obtained from the solutions of the Gross–Pitaevskii equation, the differences of both quantitative and qualitative nature are observed. So for $\delta(t)$ various exponents for time dependences are obtained. In addition, in most works, the exponent before the realization of the reconnection is less than after that, namely $\sim 0.3 - 0.4$ vs $\sim 0.6 - 0.7$. The qualitative and quantitative discrepancies can be associated with the different choices of the trap potentials V_{ext} in Eq. (1), as well as accounting or not the chemical potential.

2.4.2. Geometric configuration of the vortex loops before the reconnections

Let us turn to the consideration of the geometric configuration of the quantized vortices before the reconnections. The studies show that in the process of evolution the vortex loops approach to each other and their nearest elements are deformed, forming a pyramidal structure [86, 88, 96, 97, 100]. In the works [86, 88], the geometric characteristics of the pyramidal structure formed by the nearest elements of the vortex filaments are determined. At the same time, in the work [86], the vortex filament method and the Biot–Savart equation are used in the local approximation, and in the work [88] the Gross–Pitaevskii equation is solved numerically. The data obtained in them are quantitatively inconsistent with each other. In particular, the angles at the top of the pyramidal structure (adjacent to the nearest points of the vortices) are 61° and 112° [88], in contrast to 25° and 115°–135° obtained in [86]. In the work [97], the temperature dependence of the angles at the top of the pyramidal structure is obtained in the frame of the vortex filament method using the full Biot–Savart equation. The values of angles obtained at zero temperature agree with good accuracy with the values obtained in [86]. The study of the dynamics of the pyramidal structure of the approaching vortex filaments showed that immediately before reconnection the angles at the apex of the pyramidal structure do not change with time and practically do not depend on the temperature and the initial conditions [97]. In addition, their values correspond to the values of the angles at zero temperature. This phenomenon is due to the fact that when the vortex loops are directly approached, the forces associated with their mutual influence begin to dominate over the forces associated with the interaction of the vortex loops with the normal component of helium.

It is also worth noting that when performing the reconnection, the approaching segments of the vortex filaments are reoriented so that the direction of their circulation vectors is opposite [97]. This circumstance is very important, because, in order to preserve a helicity, the direction of the circulation of these segments must be antiparallel, as noted, for example, in the works [101, 102].

In general, in the existing works there is no disagreement on the dynamics of the formation of pyramidal structures in the vicinity of the point of reconnection. In the obtained results there are some differences in the values of the angles at the apex of the pyramidal structures, which, most likely, is associated with the different methods of the studying of the reconnecting vortex loops.

With further evolution, the rapidly approaching kinks intersect at the apex of the pyramidal structure. At their intersection, the reconnection is occured.

2.5. Evolution of the vortex loops after the reconnection

The reconnection leads to a change in the topology of the vortex system. As a rule, from the two vortex loops, the one larger vortex loop is formed. However, under certain initial conditions, the one or several additional smaller loops [89, 98] may form. As shown in these works, such a scenario is realized when the angle between the planes in, which the vortex loops are located, is sufficiently small before the reconnection. In this case, small loops subsequently quickly move away from the place of their origin or quickly collapse at a nonzero temperature. A significant deformation forms during the reconnection of the loop leads to a rapid mutual divergence of the loop elements located near the point of reconnection. As mentioned above, the divergence of the nearest elements occurs according to the root law (8). In this case, the coefficients A after reconnection take on larger values than before the reconnection. In addition, the Kelvin waves are induced during reconnection. Subsequently, they propagate along the formed loops.

2.5.1. Dynamics and properties of the vortex loops after the reconnection

Let us consider the dynamics and properties of the vortex loops after the reconnection: the average radius of curvature, the total kinetic energy of the liquid, the power of energy dissipation due to the force of mutual friction, and the vortex momentum. We know of two works in which these issues are considered in detail — these are the works [94] and [103]. In these works, the simulation of the dynamics of the vortex loops are carried out on the basis of the vortex filament method using the full Biot–Savart equation. In the field of reconnection, the vortex loop can evolve according to two main scenarios, depending on temperature. The first scenario is realized at the temperatures close to absolute zero, the second is realized at the higher temperatures.

At the temperatures close to absolute zero, the normal component of the liquid is practically absent, and, therefore, there is an absent the force of mutual friction. In this regard, the conservation of the kinetic energy and the vortex momentum of the loop should be expected, which are obtained in the works [94, 103]. The conservation of these quantities leads to the fact that the vortex loop, after the reconnection, moves with a constant average velocity. However, the conservation of the energy and momentum also means that the Kelvin waves generated during the reconnection are not damped. Moreover, these wave disturbances propagating along the vortex loop form a periodic structure, which is associated both with the involvement of new points of the loop in the additional motion and its deformation. It is also worth noting that the mean radius of curvature (see Fig. 2(a), [103]) and the length of the vortex loop are conserved, as was established in [103]. This circumstance testifies to the motion of the generated disturbances with the preservation of their structure (see Fig. 3, [104]).

At an elevated temperature of the system, the vortex loops shrink and collapse under the action of the force of mutual friction, in turn, and the Kelvin waves on the vortex loops are decay (see Fig. 4, [104]). Two characteristic stages in the evolution of the vortex loops can be distinguished here.

At the first stage, there is an increase in the radius of curvature [see Fig. 2(b) and 2(c)] and the characteristic distance between disturbances, as well as a rapid decrease in the length of the vortex loop [103]. This process is associated with the relaxation and redistribution of disturbances that arose before and immediately during the reconnection. In addition, at this stage, there is a sharp decrease in the total kinetic energy due to the action of the force of mu-

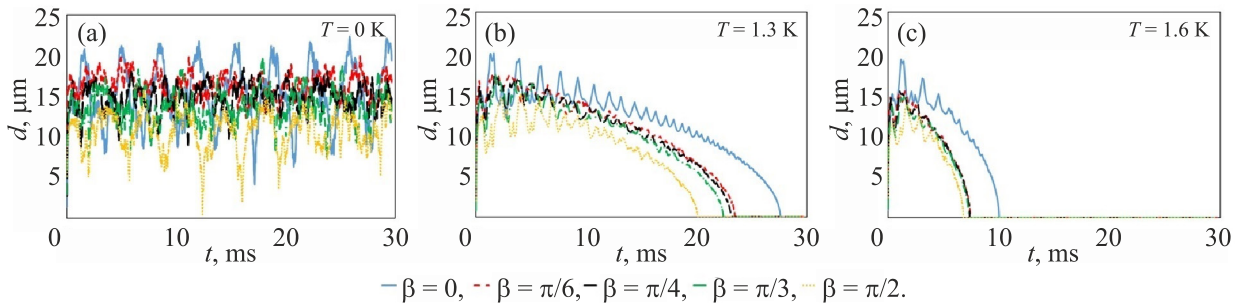

Fig. 2. (Color online) Average radius of curvature of the vortex configurations for the different initial angles between the loop planes and temperatures.

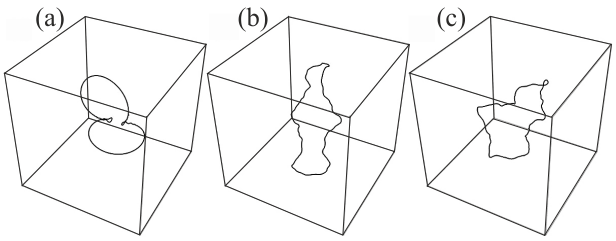

Fig. 3. An example of the vortex configurations at different times, s: 0 (a), $1.5\cdot10^{-3}$ (b), and $3\cdot10^{-3}$ (c). The initial angle between the planes of the loops is $\pi/2$. The helium temperature is close to absolute zero.

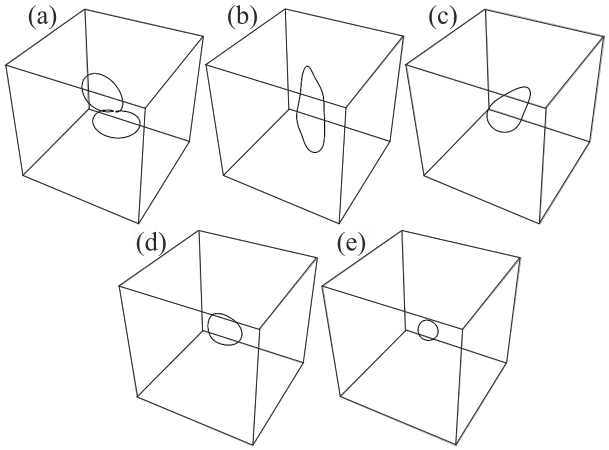

Fig. 4. An example of the vortex configurations at different times, s: 0 (a), $6\cdot10^{-4}$ (b), $1.2\cdot10^{-3}$ (c), $1.8\cdot10^{-3}$ (d), and $2.4\cdot10^{-3}$ (e). The initial angle between the planes of the loops is $\pi/2$. The helium temperature is 1.9 K.

tual friction, which is confirmed by the increased energy dissipation [94, 103]. In this case, the ratio of the total kinetic energy to the length of the vortex loop remains almost constant [103], i.e., the kinetic energy decreases in proportion to the length of the filament (as in the case of a straight vortex line) [see Fig. 5(a)].

The next stage is characterized by the fact that the redistributed disturbances begin to attenuate actively. The decrease in the average radius of the curvature is found to be proportional to the root of the time [see Fig. 2(b) and 2(c)]. Moreover, at this stage, both the length of the vortex loops and the characteristic distance between the disturbances [103] decrease as the square root of time. The observed relationships do not depend on the initial mutual arrangement of the loops. These are similar to the relationships for a single vortex ring [105]. This behavior is associated with the damping of the disturbances propagating along the vortex loop, the compression of the vortex loop and its transformation into a vortex ring. The force of mutual friction between the vortices and the normal component of superfluid helium is responsible for all these processes. This assumption is confirmed by the faster decay of the arisen disturbances and the accelerated compression of the vortex loops with an increase of the system temperature, and, as a consequence, the friction force. At this stage, the power of the energy dissipation is practically constant, and the total energy decreases linearly [103] [see Fig. 5(a) and 5(b)]. This circumstance also indicates that the dissipation of the energy is due to the force of mutual friction, and the kinetic energy of the liquid directly converts into thermal energy. In this case, the ratio $E(t)/l$ [see Fig. 5(c)] gradually begins to grow, which indicates the end of the redistribution of disturbances.

Thus, the dynamics of the vortex loops is determined by two main factors: the initial conditions and the temperature. The initial conditions determine the size and number of the disturbances arising after the reconnection, and the temperature determine the rate of their relaxation. The boundary between the observed intervals can be conditionally associated with the moment when the process of compression of the vortex loop under the action of the friction force from the normal component of superfluid helium begins to dominate over the process of the redistribution of the vortex disturbances [103].

3. Energy spectra of the velocity fields created by the various vortex configurations

The energy spectrum shows the distribution of a kinetic energy on the various scales. One of the reasons for studying the energy spectrum is that a set of the quantized vortex lines can imitate the classical turbulence. In a number of the experiments, there is a similarity between the properties of

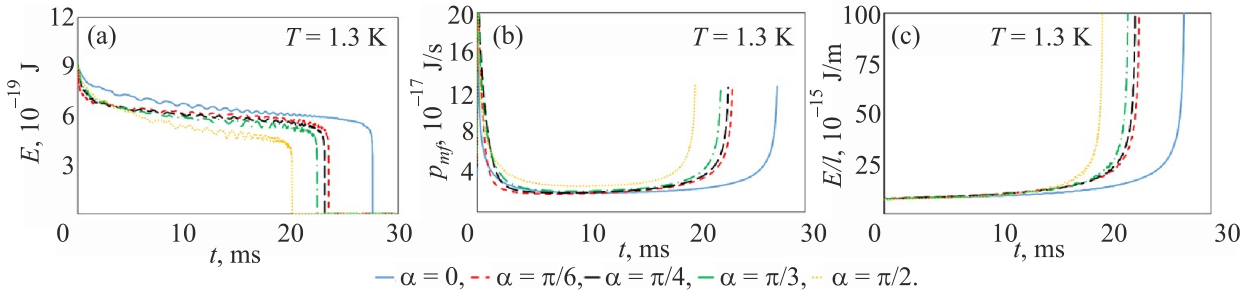

Fig. 5. (Color online) Time dependencies of the total kinetic energy (a), the power of energy dissipation due to the force of mutual friction (b), the ratio of the total kinetic energy to the size of the vortex loop (c) at a temperature $T = 1.3$ K and various angles between the initial planes of the loops.

a quantum turbulence and of the vortices in a classical fluid. For example, the experiments on the decay of a vortex tangle [106–109] show the semiclassical behavior of a quantum turbulence. To date, there is no clear explanation for this. The obtained numerical results of the study of the quantum turbulence decay [110, 111] using the Hall–Vinen–Bekarevich–Khalatnikov equations (6) demonstrate the Kolmogorov spectrum. In this case, the vortex line density decreases with time as follows, $\mathcal{L} \propto t^{-3/2}$.

The decay of quantum turbulence is investigated in the framework of the vortex filament method [112, 113] as well as in the framework of the Gross–Pitaevskii equation for the Bose–Einstein condensate [114–116]. In these works, the Kolmogorov spectrum is also obtained. A numerical study of the decay of a vortex tangle is carried out in the work [117]. It is shown that at zero temperature the decay of a concentrated dense vortex tangle in the infinite space is caused by the escape of small loops from the tangle. In the presence of the walls the vortices mainly "die" on them. On the other hand, as follows from the Vinen equation (5), during the free decay, the density of the vortex tangle decreases according to the following dependence $\mathcal{L} \propto t^{-1}$. The similar behavior of the density of the vortex tangle is observed both in the experiments and in the calculations [118–121]. A comparative analysis of these studies is carried out in the works [20, 122–124]. These studies are related to the study of the decay of a dense vortex tangle. It should be noted that the Kolmogorov spectrum is observed when the vortex tangle becomes rarefied. In this case, the vortex tangle is a set of the weakly interacting vortex loops. The another purpose of this work is to consider the energy spectrum before and after reconnection of the vortex loops. Possibly, a detailed study of the interaction of the several vortex loops will be explain the similarity of the behavior of quantum and classical turbulence.

3.1. Methods for calculating the spectrum of the velocity field

The spectrum of the velocity field can be calculated by the various methods. In addition to the direct Fourier transform, knowing the configuration of the vortex structure, it is possible to determine the energy spectrum of the system. The energy of the fluid E in the presence of the vortex filaments $\mathbf{s}(\xi)$ is determined by the following expression [125]:

$$E = \left\langle \frac{\rho_s}{2} \iiint \mathbf{v}_s^2(x,y,z)dxdydz \right\rangle = \int_0^\infty E(k)dk =$$

$$= \int_k \frac{d^3\mathbf{k}}{4\pi k^2} \left\langle 2\pi\rho_s\kappa^2 \int_0^{\mathcal{L}}\int_0^{\mathcal{L}'} s'(\xi_1)s'(\xi_2)\, e^{i\mathbf{k}(\mathbf{s}(\xi_1)-\mathbf{s}(\xi_2))} d\xi_1 d\xi_2 \right\rangle.$$

Hence, the kinetic energy spectrum is determined as follows:

$$E(k) = \frac{\rho_s\kappa^2}{2(2\pi)^3} \int_k \frac{d\Omega_k}{|k|^2} \int_0^{\mathcal{L}}\int_0^{\mathcal{L}'} s'(\xi_1)s'(\xi_2)\, e^{i\mathbf{k}(\mathbf{s}(\xi_1)-\mathbf{s}(\xi_2))} d\xi_1 d\xi_2,$$

where $d\Omega_k = k^2 \sin\theta_k d\theta_k d\Phi_k$ is the elementary volume in the spherical coordinates. In the isotropic case, the spectral density is determined by the following expression [126]:

$$E(k) = \frac{\rho_s\kappa^2}{(2\pi)^2} \int_0^{\mathcal{L}}\int_0^{\mathcal{L}'} \frac{\sin(k\,|\,\mathbf{s}(\xi_1)-\mathbf{s}(\xi_2)\,|)}{k\,|\,\mathbf{s}(\xi_1)-\mathbf{s}(\xi_2)\,|} d\mathbf{s}(\xi_1)\cdot d\mathbf{s}(\xi_2). \quad (11)$$

The another method for the determining of the spectral density is the statistical approach [9, 127]. To find the spectrum, the velocity field must first be determined. Then it is required to calculate the velocity correlators:

$$S_2^{\parallel}(l) = \left\langle \left(\left[\mathbf{v}(\mathbf{r}+\mathbf{l})-\mathbf{v}(\mathbf{r})\right]\cdot\frac{\mathbf{l}}{l} \right)^2 \right\rangle,$$

$$S_2^{\perp}(l) = \left\langle \left(\left[\mathbf{v}(\mathbf{r}+\mathbf{l})-\mathbf{v}(\mathbf{r})\right]\times\frac{\mathbf{l}}{l} \right)^2 \right\rangle. \quad (12)$$

The angle brackets mean an averaging over the ensemble, that is, over all pairs of the points separated by the distance l, for the all possible values of r. The dependencies

$$S_2^{\parallel}(l) \propto S_2^{\perp}(l) \propto l^{\alpha}$$

in the coordinate space ones corresponds the dependence

$$E(k) \propto k^{-m}$$

in the space of the wave numbers ($m = \alpha + 1$) [9, 127]. From the dimensional considerations Kolmogorov [128] for the longitudinal and transverse structure functions of the second order obtained:

$$S_2^{\parallel}(l) \propto S_2^{\perp}(l) \propto \varepsilon^{2/3} l^{2/3}.$$

This is the famous "two-thirds" law. In the space of wave numbers, this expression corresponds to:

$$E(k) \propto k^{-\alpha-1} = k^{-5/3}.$$

3.2. Energy spectra of the velocity fields created by the vortices before a reconnection

Before the moment of a reconnection, the kinks are formed on the vortex loops (lines) (see Fig. 1). As is noted above the time dependence of the minimum distance between the elements of vortex loops is closely related to the reconnection rate, and the geometric parameters of the kinks play a decisive role in the formation of the three-dimensional velocity field induced by the reconnecting vortices.

In the work [124] it is assumed that exactly the reconnection processes are responsible for the fact that the energy spectrum in a quantum liquid is similar to that in a classical liquid. The quantum vortices can not stretch and contract, unlike the classical ones. At the time of the reconnection, the part of a vortex filament is "burned out", that mimics the energy transfer into a tiny area near the point of a collapse. In a classical liquid, the vortex stretching plays a similar role in the energy transfer into small scales. Today,

both in the quantum and classical fluids an exact geometric shape $s(\xi)$ of the vortex lines before a reconnection is not obtained analytically. An asymptotic solution of the dynamics of the quantum vortex loops just before the reconnection is obtained in [100]. Using this solution and the Eq. (11) to calculate the energy spectrum the dependence $E(k)$ is obtained in the work [124] numerically. Further, using the asymptotic expansion method [129] the integral (11) is roughly estimated at large k. As a result, the spectrum $E(k)$ was obtained analytically. Both obtained curves are shown in Fig. 6 [84]. As you can see from Fig. 6 in either case $E(k) \propto k^{-\alpha-1} = k^{-5/3}$. This circumstance allowed the authors of this work to connect the possible cause of the appearance of the Kolmogorov spectrum with the shape of the reconnecting vortex filaments. The obtained dependence $E(k)$ is approximate, since it is based on an asymptotic solution. The spectrum $E(k)$ is valid only on small scales. On a large scale, the energy spectrum should be obtained by integrating the formula (11) over the entire vortex configuration, including the very distant elements of the vortex line. It is clear that this can be done in the case where a large-scale organization of the structure of the vortex tangle is known (at least in the statistical sense).

In the work [84], using the vortex filament method and the full Biot–Savart equation, the configurations of the vortex filaments was obtained before the reconnections. Using a statistical method (12), the spectrum of the velocity field induced by the different configurations of the quantum vortex filaments was obtained. These configurations were obtained at the various time before the reconnections. The spectrum were obtained on the scales of the order of the sizes of the pyramidal structures. In Fig. 7 the obtained dependences of the second order longitudinal correlation functions on l are presented. Note that the notation $S_2^{\parallel}(l) = C_{ll}(l)$ given in the various papers are equivalent.

It is shown in [84] that the small changes in the loop configurations lead to the rather significant changes in the $E(k)$ dependence. In the same work, the influence of the spatial inhomogeneity (kink) on the energy spectrum on the scales larger than the kink itself is determined. For this, the second order structure function was calculated in the region where both vortex loops were located before the reconnection. The obtained result of the C_{ll} is shown in Fig. 8.

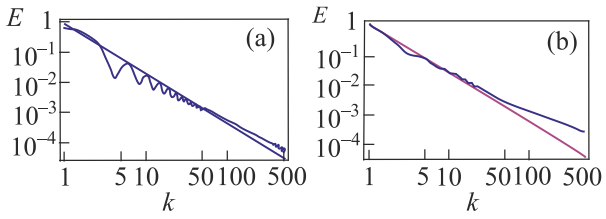

Fig. 6. (a) Spectrum $E(k)$ is obtained analytically. (b) Spectrum $E(k)$ is obtained numerically. The straight line has a slope of 5/3.

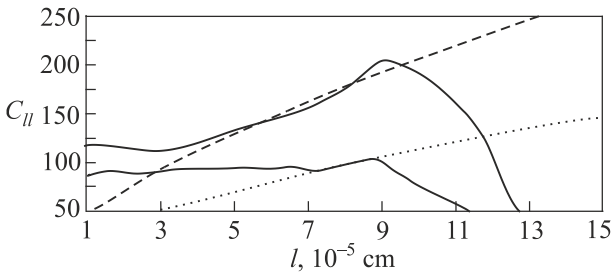

Fig. 7. Dependences of the second order longitudinal correlation functions on l. Solid lines are the dependence of the structure functions of the velocity fields in the vicinity of the kink on the scale l. The dashed and dotted lines are some functions proportional to $l^{2/3}$. The upper solid line corresponds to the vortex configuration closer to the reconnection point than the lower one.

From Fig. 8 it follows that on the scales of the order of the kink size is $C_{ll}(l) \propto l^{0.6}$ and $E(k) \propto k^{-1.6}$. On the large scales $C_{ll}(l) \propto l^{0,45}$ and $E(k) \propto k^{-1.45}$. On the scales of the order of the characteristic vortex size $C_{ll}(l) \propto l^{-3}$, that corresponds to $E(k) \propto k^2$. It is the energy spectrum from a straight line on the small k.

The results of the studies considered above show that the Kolmogorov energy spectrum is observed on scales of the order of pyramidal structures formed as a result of the intense interaction of vortex filaments before the reconnection. On smaller scales, an observed spectrum corresponds to the spectrum produced by a smooth vortex filament. Thus, a single kink-type inhomogeneity cannot create a velocity field with a spectrum similar to the Kolmogorov spectrum, especially on the scale of the system. However, in all considered cases, the presence of kinks leads to characteristic features in the energy spectrum. It should be expected that the presence of many kinks, for example, in a dense vortex tangle characterized by a large number of reconnections (reconnection rate $\frac{dN_r}{dt} \propto \mathcal{L}^{5/2}$ [19]) could create a Kolmogorov-type spectrum.

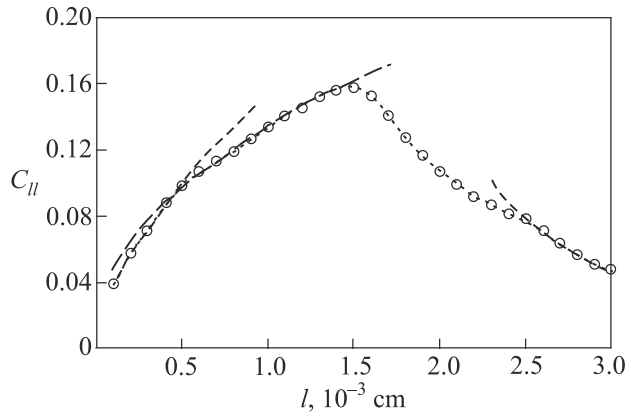

Fig. 8. Structural function for a system of the two interacting vortex loops initially lying in the same plane. The structure function corresponds to the dotted line with round markers. Dashed lines are power approximations: $l^{0.6}$, $l^{0.45}$, l^{-3} on the corresponding scales l.

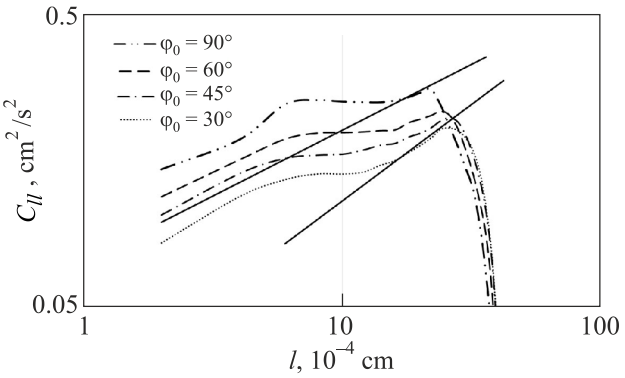

Fig. 9. Dependence of the structure functions on l before reconnection for the different initial angles between the loop planes.

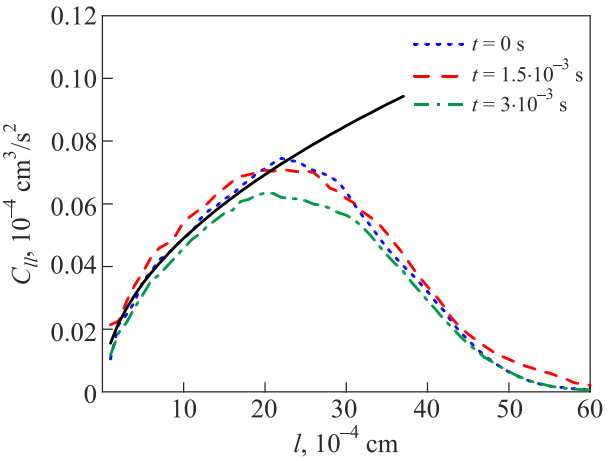

Fig. 10. Longitudinal structure functions of the velocity fields corresponding to the vortex configurations Fig. 3. The black solid line is the approximating curve $C_{ll}(l) \propto l^{1/2}$. In k space, this dependence corresponds to the energy spectrum: $E(k) \propto k^{-3/2}$.

On scales of the order of the characteristic sizes of the vortex loops in the work [130] the spectral characteristics of the velocity fields generated by the different configurations of the vortex loops were calculated before the reconnection.

The configurations differed from each other in the initial arrangement of the planes in which the vortex loops were located, see Fig. 9. The slope of the approximating tangents (solid lines in Fig. 9) increases with the decreasing of the angle between the planes of the original position of the loops. It turned out that the angles of the slope longitudinal structural function of the second order C_{ll}. $C_{ll}(l)$ vary in the range from 0.45 to 0.66, which corresponds to the spectra $E(k) \propto k^{-1.45}$ and $E(k) \propto k^{-5/3}$, $E(k) \propto k^{-1.45}$ and $E(k) \propto k^{-5/3}$.

Thus, during reconnection vortex loops can create a velocity field with spectral characteristics close to the Kolmogorov spectrum, at least in a certain range of wavenumbers k.

3.3. Energy spectra of the velocity fields created by the vortices after the reconnection

In the work [104], using the statistical method, the nature of the energy spectrum of the velocity fields corresponding to the moving vortex loops formed after the reconnection of two vortex loops was determined. The numerical studies were carried out at the various temperatures and initial arrangements of the vortex rings. The dynamics of the vortex loops was obtained within the framework of the vortex line method using the full Biot–Savart equation. It turned out to be surprising that in all cases the structure functions of the second order have the same form $C_{ll}(l) \propto l^{1/2}$. In the k space, this dependence corresponds to the energy spectrum $E(k) \propto k^{-3/2}$, that is a spectrum of a smooth vortex ring.

At zero temperature, the spectral characteristics of the vortex loops do not change over time due to the absence of energy dissipation. The only difference is that the amplitudes of the structure functions of the second order is somewhat different for the different initial conditions, that corresponds to the presence of various perturbations arising on the vortex loops during reconnections. The configurations of the vortex loops at the temperature near absolute zero at the different times are given in Fig. 10. For these configurations, Fig. 10 shows the dependences of the longitudinal structure functions of the second order from the scale l.

The numerical results of the influence of the initial conditions are shown in Fig. 11(a).

As you can see from this figure, the initial data do not affect the power exponent α. The influence of temperature also does not affect the values of the exponent $S_2^{\parallel}(l)$ as shown in Fig. 11(b).

Moreover, the longitudinal structural functions of the second order do not change when the vortex loop collapses. The amplitudes of the structure functions decrease with the temperature, which corresponds to a higher rate of energy dissipation. The mechanism of the vortex loops decay is similar to the decay of the mechanism of the single smooth vortex rings. The perturbations arising during the reconnection somewhat can speed up this process [105].

4. Summary

On the whole, most of the existing results concerning the dynamics of reconnecting loops are in qualitative agreement with each other. Thus, the dependence of the minimum distance between the elements of the vortex loops before reconnection has a root form. The divergence of the nearest elements of the vortex loop after the realization of reconnection also occurs according to the root law, but several times faster. The specific values of the obtained coefficients are somewhat inconsistent with each other, which may be due to the consideration of the different time intervals, as well as the different initial conditions. In addition, today there is no disagreement regarding the geometric configuration of the vortex loops before the reconnection — the sections of the threads near the point of reconnection are oriented antiparallel to each other, and the elements

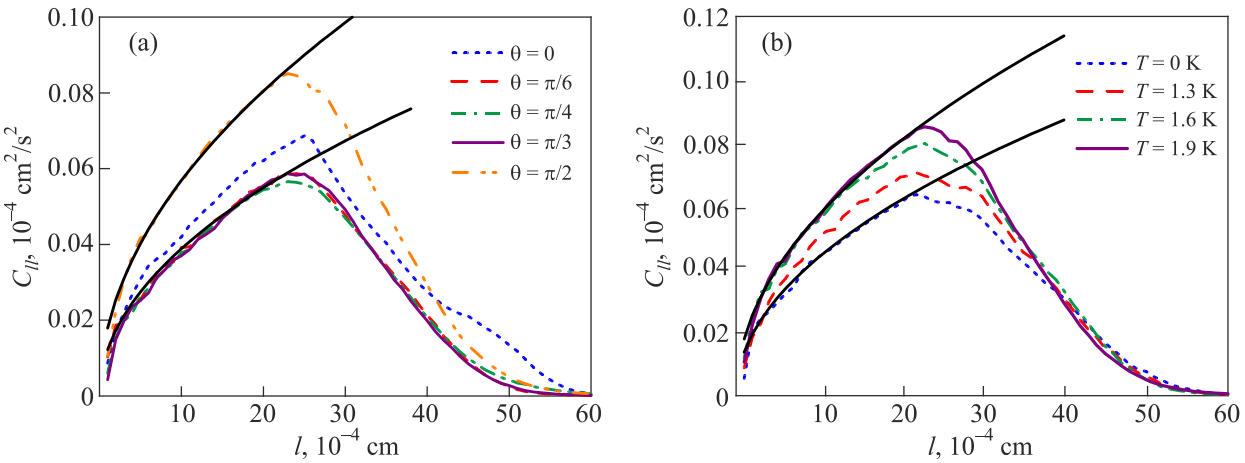

Fig. 11. (a) Structural functions of the velocity fields corresponding to the configurations of the vortex loops after reconnection at different initial angles between the planes of the loops. (b) Structure functions of the velocity fields for the vortex loops at different temperatures. The fluid temperature is 1.9 K, t = 0 s.The angle between the initial planes of the loops is $\pi/2$. Black solid lines — approximating curves $C_{ll}(l) \propto l^{1/2}$. In k space, this dependence corresponds to the energy spectrum: $E(k) \propto k^{-3/2}$.

adjacent to them form a pyramidal structure. The number of works considering the properties of reconnecting vortex loops is significantly less than the number of works considering their dynamics. However, even here in the available works, there are no significant divergences. At zero temperature, the vortex loops continue to move with the preservation of their properties, and the Kelvin waves generated during reconnection propagate along with the vortex loops without dumping. At elevated temperatures, due to the force of mutual friction, the vortex loops collapse, and the Kelvin waves generated during reconnection rapidly decay. These processes are accelerated with the temperature increasing.

One of the main remaining open questions is the question of the role of the reconnecting vortex loops in the formation of the turbulent spectrum. The other mechanisms may be responsible for the formation of the turbulent spectrum. So, for example, in many of the numerical studies carried out near absolute zero, at the end of the decay of a vortex tangle, the remained vortex loops and lines begin and end usually on the walls of the experimental cell. The Kelvin waves or the solitons are formed along these lines during their dynamics. The paper [30] discusses the role of such waves and solitons in a vortex system. It is assumed that "a turbulent vortex tangle in the limit of zero temperature can be represented as a gas of solitons and Kelvin waves on the vortex lines interacting with a gas of the vortex rings and photons in the bulk — with frequent interconversion of the ring into solitons and vice versa" [30].

The statistical properties of quantum turbulence are also being studied experimentally. Thus, in the works [27, 131], the transverse structure functions of the second order are found, which made it possible to determine the spectrum of the vortex tangle. In numerical studies of the spectral characteristics of the vortex loop after reconnection [104] and the vortex ring [105], similar results are obtained. The [131] experiment shows the dependence of the index of the structural functions on external parameters: the temperature and the counterflow velocity. In stationary situations, the dependences were obtained, respectively, in k space $E(k) \propto k^{-m}$, $m > 1.88$ ($m = \alpha + 1$). It is found that the values of the index α increase with increasing the heat flux density. When the temperature of the liquid changes, the index α changes; it can decrease or increase depending on the value of the heat flux density. In the work [28], a semi-quantitative theory of stationary, homogeneous, isotropic turbulence developed in the presence of counterflow. The results of the developed theory are compared with the experimental results [131]. Good qualitative agreement is found between theory and observations for T = 1.85 K [131].

In the work [130], the spectrum of the vortex tangles arising in the counterflow of the superfluid and normal components of helium is also investigated by the method of the structure functions. The vortex configurations are obtained by the vortex filament method using the full Biot–Savart equation. The results are obtained at the various values of the counterflow velocities from 0.3 cm/s to 1.2 cm/s and the temperatures from 1.3 to 1.9 K. As a result, it is found that an increase in the counterflow velocity leads to an increase in the dissipation rate, but does not affect the nature of the spectrum. Note that the obtained results in this work do not agree with the results of the [131] experiment. In turn, that the temperature increase leads not only to an increase in the rate of energy dissipation but also affects on the spectral characteristics of the system on the intervortex scale. The energy spectra show different power law: $E(k) \sim k^{-1.3}$, $E(k) \sim k^{-1.35}$, and $E(k) \sim k^{-1.4}$, m = = 1.3, 1.35, 1.4, respectively. Monotonicity is observed in the increase in the modulus of the exponent with increasing temperature. On large scales, the spectrum $E(k) \sim k^{-1}$ is observed for all considered temperatures. Note that in the experiment [131] $m > 1.88$. An increase in the index with an increase in the temperature is associated with an increase in

the number of the reconnections, since kinks near the reconnection point can create a velocity field with spectral characteristics close to Kolmogorov's. Accordingly, the reconnections can possibly play a significant role in the formation of quantum turbulence, at least on the intervortex scales.

In connection with the development of new methods for the experimental study of the quantum vortex filaments, it will become possible soon to determine the validity of the developed models and hypotheses, as well as to establish the mechanism responsible for the formation of the turbulent spectrum: the vortex loops, the solitons, the Kelvin waves, the reconnections, or something else.

1. F. London, *Nature* **141**, 643 (1938).
2. F. London, *Phys. Rev.* **54**, 947 (1938).
3. F. London, *Superfluids*, Wiley, New York (1954), Vol. 2, p. 70.
4. L. Tisza, *Nature* **141**, 913 (1938).
5. L. Tisza, *Phys. Rev.* **72**, 838 (1947).
6. L. D. Landau, *JETP* **11**, 592 (1941).
7. L. D. Landau, *JETP* **14**, 112 (1944).
8. L. Landau, *Phys. Rev.* **75**, 884 (1949).
9. L. D. Landau and E. M. Lifshitz, *Fluids Mechanics*, Oxford: Pergamon Press (1987).
10. E. L. Andronikashvili, *JETP* **16**, 780 (1946).
11. C. J. Gorter and L. H. Mellink, *Physica* **15**, 285 (1949).
12. G. Gamota, *Phys. Rev. Lett.* **31**, 517 (1973).
13. B. M. Guenin and G. B. Hess, *J. Low Temp. Phys.* **33**, 243 (1978).
14. S. I. Davis, P. C. Hendry, and P. V. E. McClintock, *Physica B* **280**, 43, (2000).
15. Michael Niemetz, Hurbert Kerscher, and Wilfried Schoepe, *J. Low Temp. Phys.* **126**, 287 (2002).
16. P. M. Walmsley, A. I. Golov, H. E. Hall, A. A. Levchenko, and W. F. Vinen, *Phys. Rev. Lett.* **99**, 265302 (2007).
17. S. K. Nemirovskii, *Phys. Rep.* **524**, 85 (2013).
18. Makoto Tsubota, Michikazu Kobayashi, Hiromitsu Takeuchi, *Phys. Rep.* **522**, 191 (2013).
19. L. Kondaurova, V. L'vov, A. Pomyalov, and I. Procaccia, *Phys. Rev. B* **89**, 014502 (2014).
20. C. F. Barenghi, V. S. L'vov, and P. E. Roche, *Proc. Natl. Acad. Sci. USA* **111**, 4683 (2014).
21. C. F. Barenghi, L. Skrbek, and K. P. Sreenivasan, *Proc. Natl. Acad. Sci. USA* **111**, 4647 (2014).
22. Wei Guo, Marco La Mantiac, Daniel P. Lathropd, and Steven W. Van Sciver, *Proc. Natl. Acad. Sci. USA* **111**, 4653 (2014).
23. Risto Hanninen and Andrew W. Baggaley, *Proc. Natl. Acad. Sci. USA* **111**, 4667, (2014).
24. Paul Walmsley, Dmitry Zmeev, Fatemeh Pakpour, and Andrei Golov, *Proc. Natl. Acad. Sci. USA* **111**, 4691, (2014).
25. D. E. Zmeev, P. M. Walmsley, A. I. Golov, P. V. E. McClintock, S. N. Fisher, and W. F. Vinen, *Phys. Rev. Lett.* **115**, 155303 (2015).
26. R. Hanninen, *Phys. Rev. B* **92**, 184508 (2015).
27. A. Marakov, J. Gao, W. Guo, S. W. Van Sciver, G. G. Ihas, D. N. McKinsey, and W. F. Vinen, *Phys. Rev. B* **91**, 094503 (2015).
28. Victor S. L'vov and Anna Pomyalov, *Phys. Rev. B* **97**, 214513 (2018).
29. Luca Galantucci, Andrew W. Baggaley, Carlo F. Barenghi, and Giorgio Krstulovic, *Eur. Phys. J. Plus.* **135**, 547 (2020).
30. W. Guo and A. I. Golov, *Phys. Rev. B* **101**, 064515 (2020).
31. P. J. Green,· M. J. Grant, J. W. Nevin, P. M. Walmsley, and A. I. Golov, *J. Low Temp. Phys.* **201**, 11 (2020).
32. S. K. Nemirovskii, *Int. J. Thermophys.* **26**, 476 (2017).
33. L. Biferale, D. Khomenko, V. L'vov, A. Pomyalov, I. Procaccia, and G. Sahoo, *Phys. Rev. B* **95**, 184510 (2017).
34. L. P. Pitaevskii and S. Stringari, *Bose–Einstein Condensation*, Oxford University Press (2003).
35. E. A. L. Henn, J. A. Seman, G. Roati, K. M. F. Magalhaes, and V. S. Bagnato, *Phys. Rev. Lett.* **103**, 045301 (2009).
36. S. P. Johnstone, A. J. Groszek, P. T. Starkey, C. J. Billington, T. P. Simula, and K. Helmerson, *Science* **364**, 1267 (2019).
37. J. Skipp, V. L'vov, and S. Nazarenko, *Phys. Rev. A* **102**, 043318 (2020).
38. V. G. Rousseau, G. G. Batrouni, D. E. Sheehy, J. Moreno, and M. Jarrell, *Phys. Rev. Lett.* **104**, 167201 (2010).
39. H. Deng, H. Haug, and Y. Yamamoto, *Rev. Mod. Phys.* **82**, 1489 (2010).
40. T. Byrnes, N. Y. Kim, and Y. Yamamoto, *Nat. Phys.* **10**, 803 (2014).
41. Wei Baoa, Xiaoze Liua, Fei Xueb, Fan Zhenge, Renjie Taoa, Siqi Wanga, Yang Xiaa, Mervin Zhaoa, Jeongmin Kima, Sui Yanga, Quanwei Lia, Ying Wanga, Yuan Wanga, Lin-Wang Wange, Allan H. MacDonaldb, and Xiang Zhanga, *Proc. Natl. Acad. Sci. USA* **116**, 2027, (2019).
42. I. Carusotto and C. Ciuti, *Quantum fluids of light*, *Rev. Mod. Phys.* **85**, 299 (2013).
43. A. J. E. Kreil, D. A. Bozhko, H. Y. Musiienko-Shmarova, V. I. Vasyuchka, V. S. L'vov, A. Pomyalov, B. Hillebrands, A. A. Serga, *Phys. Rev. Lett.* **121**, 077203 (2018).
44. L. Mihalceanu, D. Bozhko, V. Vasyuchka, A. A. Serga, B. Hillebrands, A. Pomyalov, V. L'vov, and V. Tyberkevych, *Ukr. J. Phys.* **64**, 927 (2019).
45. A. I. Golov, P. M. Walmsley, and P. A. Tompsett, *Charged Tangles of Quantized Vortices in Superfluid* ^{4}He, *J. Low Temp. Phys.* **161**, 509 (2010).
46. W. Guo, S. B. Cahn, J. A. Nikkel, W. F. Vinen, and D. N. McKinsey, *Phys. Rev. Lett.* **105**, 045301 (2010).
47. E. Fonda, K. R. Sreenivasan, and D. P. Lathrop, *Rev. Sci. Instrum.* **83**, 085101 (2012).
48. L. Pitaevskii and S. Stringari, *Bose–Einstein Condensation and Superfluidity*, Oxford University Press (2016).
49. K. W. Schwarz, *Phys. Rev. B* **31**, 5782 (1985).
50. K. W. Schwarz, *Phys. Rev. B* **38**, 2398 (1988).
51. L. P. Pitaevskii, *Adv. Phys. Sci.* **168**, 641 (1998).
52. A. J. Allen, E. Zaremba, C. F. Barenghi, and N. P. Proukakis, *Phys. Rev. A* **87**, 013630 (2013).
53. S. Stringar, *JETP* **154**, 964, (2018).

54. D. W. Moore and P. G. Saffman, *Philos. Trans. R. Soc. A* **272**, 403 (1972).
55. P. G. Saffman, *Stud. Appl. Maths*. **49**, 371 (1970).
56. P. G. Saffman and G. R. Baker, *Annu. Rev. Fluid Mech.* **11**, 95 (1979).
57. R. G. M. Aarts, *A Numerical Study of Quantized Vortices in He II*, Tech. Univer. Eindhoven (1993).
58. D. C. Samuels, *Phys. Rev. B* **46**, 11714 (1992).
59. A. T. A. M. de Waele and R. G. K. M. Aarts, *Phys. Rev. Lett.* **72**, 482 (1994).
60. D. C. Samulels and D. Kivotides, *Phys. Rev. Lett*. **83**, 5306 (1999).
61. L. P. Kondaurova and S. K. Nemirovskii, and M. V. Nedoboiko, *Simulation of Stochastic Vortex Tangle*, *Fiz. Nizk. Temp.* **29**, 835 (2003) [*Low Temp. Phys.* **29**, 624 (2003)].
62. H. Adachi, S. Fujiyama, and M. Tsubota, *Phys. Rev. B* **81**, 104511 (2010).
63. M. Tsubota, T. Araki, and S. K. Nemirovskii, *Physica B* **284**, 79 (2010).
64. D. Kivotides, *J. Fluid Mech*. **668**, 58 (2011).
65. W. F. Vinen, *Proc. R. Soc. Lond. A* **240**, 114 (1957).
66. W. F. Vinen, *Proc. R. Soc. Lond. A* **240**, 128 (1957).
67. W. F. Vinen, *Proc. R. Soc. Lond. A* **242**, 493 (1957).
68. W. F. Vinen, *Proc. R. Soc. Lond. A* **243**, 400 (1958).
69. S. K. Nemirovskii and V. V. Lebedev, *JETP* **84**, 1729 (1983).
70. K. Yamada, S. Kashiwamura, and K. Miyake, *Physica B* **154**, 318 (1989).
71. J. A. Guerst, *Physica B* **154**, 327 (1989).
72. Luiza Kondaurova, Victor Efimov, and Alexey Tsoi, *J. Low Temp. Phys*. **187**, 80 (2017).
73. L. P. Kondaurova, *Dynamics of Vortex Lines Density and Heat Transfer Processes in Superfluid Helium*, *Fiz. Nizk. Temp*. **44**, 36 (2018) [*Low Temp. Phys*. **44**, 29 (2018)].
74. V. B. Efimov, A. A. Orlova, L. P. Kondaurova and A. G. Gorkun, *Heat Transfer under Pulsed Heating in Superfluid Helium*, *Fiz. Nizk. Temp*. **45**, 1158 (2019) [*Low Temp. Phys*. **45**, 988 (2019)].
75. L. P. Kondaurova, *Dynamics of the Density of Vortex Lines and Thermal Pulses in Superfluid Helium*, *Fiz. Nizk. Temp*. **46**, 693 (2020) [*Low Temp. Phys*. **46**, 579 (2020)].
76. H. E. Hall and W. F. Vinen, *Proc. R. Soc. Lond. A* **238**, 204 (1956).
77. H. E. Hall and W. F. Vinen, *Proc. R. Soc. Lond. A* **238**, 215 (1956).
78. I. M. Khalatnikov, *An Introduction to the Theory of Superfluidity*, W. A. Benjamin, New York/Amsterdam (1965).
79. S. R. Stalp, L. Skrbek, and R. J. Donnelly, *Phys. Rev. Lett.* **82**, 4831 (1999).
80. W. F. Vinen, *Phys. Rev. B* **61**, 1410 (2000).
81. W. F. Vinen and J. J. Niemela, *J. Low Temp. Phys*. **128**, (2002).
82. S. K. Nemirovskii, *Macroscopic Dynamics of Superfluid Turbulence*, *Fiz. Nizk. Temp*. **45**, 986 (2019) [*Low Temp. Phys*. **45**, 841 (2019)].
83. Sergey K. Nemirovskii, *J. Low Temp. Phys*. **201**, 254 (2020).
84. V. A. Andryushchenko and S. K. Nemirovskii, *Collapsing vortex filaments and the spectrum of quantum turbulence*, *Fiz. Nizk. Temp*. **43**, 150 (2017) [*Low Temp. Phys*. **43**, 125 (2017)].
85. J. Koplik and H. Levine, *Phys. Rev. Lett*. **71**, 1375 (1993).
86. A. De Waele and R. Aarts, *Phys. Rev. Lett.* **72**, 482 (1994).
87. M. S. Paoletti, M. E. Fisher, and D. P. Lathrop, *Physica D* **239**, 1367 (2010).
88. R. Tebbs, A. J. Youd, and C. F. Barenghi, *J. Low Temp. Phys*. **162**, 314 (2011).
89. M. Kursa, K. Bajer, and T. Lipniacki, *Phys. Rev. B* **83**, 014515 (2011).
90. S. Zuccher, M. Caliari, A. W. Baggaley, and C. F. Barenghi, *Phys. Fluids* **24**, 125108 (2012).
91. A. J. Allen, S. Zuccher, M. Caliari, N. P. Proukakis, N. G. Parker, and C. F. Barenghi, *Phys. Rev. A* **90**, 013601 (2014).
92. C. Rorai, J. Skipper, R. M. Kerr, and K. R. Sreenivasan, *J. Fluid Mech*. **808**, 641 (2016).
93. A. Villois and D. Proment, *Phys. Rev. Fluids* **2**, 044701, (2017).
94. R. Hanninen, *Phys. Rev. B* **88**, 054511 (2013).
95. M. Tsubota and H. Adachi, *Simulation of Counterflow Turbulence by Vortex Filaments*, *J. Low Temp. Phys*. **162**, 367 (2011).
96. V. A. Andryushchenko, L. P. Kondaurova, and S. K. Nemirovskii, *Dynamics of Quantized Vortices Before Reconnection*, *J. Low Temp. Phys*. **185**, 377 (2016).
97. V. A. Andryushchenko, L. P. Kondaurova, and S. K. Nemirovskii, *Dynamics of Nonplanar Quantized Vortex Rings before Reconnection at Finite Temperatures*, *J. Low Temp. Phys*. **187**, 523 (2017).
98. V. A. Andryushchenko and L. P. Kondaurova, *Dynamics of Vortex Loops after Reconnection in Superfluid Helium at Different Temperatures*, *Fiz. Nizk. Temp*. **44**, 1302 (2018) [*Low Temp. Phys*. **44**, 1020 (2018)].
99. F. Hussain and K. Duraisamy, *Phys. Fluids* **23**, 021701 (2011).
100. L. Boue, D. Khomenko, V. S. L'vov, and I. Procaccia, *Analytic Solution of the Approach of Quantum Vortices Towards Reconnection*, *Phys. Rev. Lett.* **111**, 145302, (2013).
101. A. Pumir and E. D. Siggia, *Vortex Dynamics and the Existence of Solutions to the Navier–Stokes Equations*, *Phys. Fluids* **30**, 1606 (1987).
102. S. Zuccher and R. L. Ricca, *Helicity Conservation under Quantum Reconnection of Vortex Rings*, *Phys. Rev. E* **92**, 061001 (2015).
103. V. A. Andryushchenko and L. P. Kondaurova, *Energy Dissipation after Single Vortex Reconnection in He II at Different Temperatures*, *Fiz. Nizk. Temp*. **45**, 1053 (2019) [*Low Temp. Phys*. **45**, 901 (2019)].
104. V. A. Andryushchenko and L. P. Kondaurova, *The Energy Spectrum of Reconnected Vortex Loops in He II*, *Fiz. Nizk. Temp*. **46**, 1155 (2020). [*Low Temp. Phys*. **46**, 977 (2020)].
105. V. A. Andryushchenko, *Dynamics of Quantized Rings and Loops after Reconnection in Superfluid Helium*, *J. Phys. Conf. Ser.* **1382**, 012002 (2019).

106. M. R. Smith, R. J. Donnelly, N. Goldenfeld, and W. F. Vinen, *Phys. Rev. Lett.* **71**, 2583 (1993).
107. J. Maurer and P. Tabeling, *Local Investigation of Superfluid Turbulence*, *Europhys. Lett.* **43**, 29 (1998).
108. A. V. Gordeev, T. V. Chagjvets, F. Soukup, and L. Skrbek, *J. Low Temp. Phys.* **138**, 549 (2005).
109. J. Salort, B. Chabaud, E. Lévêque, and P.-E. Roche, *J. Phys. Conf. Ser.* **318**, 042014 (2011).
110. D. H. Wacks and C. F. Barenghi, *Phys Rev B* **84**, 184505 (2011).
111. J. Salort, B. Chabaud, E. Lévêque, and P.-E. Roche, *Europhys. Lett.* **97**, 34006 (2012).
112. T. Araki, M. Tsubota, and S. K. Nemirovskii, *Phys. Rev. Lett.* **89**, 145301 (2002).
113. D. Kivotides, C. J. Vassilicos, D. C. Samuels, and C. F. Barenghi, *Europhys. Lett.* **57**, 845 (2002).
114. C. Nore, M. Abid, and M. E. Brachet, *Phys. Rev. Lett.* **78**, 3896 (1997).
115. M. Kobayashi and M. Tsubota, *Phys. Rev. Lett.* **94**, 065302 (2005).
116. N. Sasa, T. Kano, M. Machida, V. S. L'vov, O. Rudenko, and M. Tsubota, *Phys. Rev. B* **84**, 054525 (2011).
117. L. Kondaurova and S. K. Nemirovskii, *Phys. Rev. B* **86**, 134506 (2012).
118. K. W. Schwarz and J. R. Rozen, *Phys. Rev. B* **44**, 7563 (1991).
119. M. R. Smith, R. J. Donnelly, N. Goldenfeld, and W. F. Vinen, *Phys. Rev. Lett.* **71**, 2583 (1993).
120. D. Kivotides, C. F. Barenghi, and D. C. Samuels, *Europhys. Lett.* **54**, 774 (2001).
121. L. Skrbek, A. V. Gordeev, and F. Soukup, *Phys. Rev.* **67**, 047302 (2003).
122. M. Tsubota, and M. Kobayashi, *Progress in Low Temperature Physics: Quantum Turbulence* (2009), Vol. 16.
123. S. K. Nemirovskii, *J. Low Temp. Phys.* **171**, 504 (2013).
124. S. K. Nemirovskii, *Phys. Rev. B* **90**, 104506 (2014).
125. S. K. Nemirovskii and W. Fiszdon, *Rev. Mod. Phys.* **67**, 37 (1995).
126. Luiza Kondaurova and Sergey K. Nemirovskii, *AIP Conference Proceedings* **850**, 223 (2006).
127. K. P. Zibin and V. A. Sirota, *Adv. Phys. Sci.* **185**, 593 (2015).
128. A. N. Kolmogorov, *Proc. R. Soc. Lond. A* **434**, 9 (1991).
129. M. V. Fedoryuk, *The Saddle-Point Method*, Nauka, Moscow (1977).
130. V. A. Andryushchenko and L. P. Kondaurova, *Energy Spectra of Counterflow Quantum Turbulence at Different Temperatures*, *Fiz. Nizk. Temp.* **43**, 245 (2017) [*Low Temp. Phys.* **43**, 200 (2017)].
131. J. Gao, E. Varga, W. Guo, and W. F. Vinen, *Phys. Rev. B* **96**, 094511 (2017).

Динаміка, властивості та спектр вихрових петель після реконнекції у надплинному гелії (Огляд)

L. P. Kondaurova, V. A. Andryushchenko

Квантова турбулентність — це сукупність взаємодіючих квантових вихрових петель та ниток. Систематизовано інформацію про поточний стан досліджень квантових вихрових петель після реконнекції у надплинному гелії: геометрія, динаміка, властивості вихрових петель, енергетичний спектр до та після реконнекції . Обговорено можливу роль реконнекції у формуванні турбулентного спектра, а також основні методи та підходи до вивчення вихрових петель після реконнекції та квантової турбулентності.

Ключові слова: надплинний гелій, вихрові петлі, реконнекція, енергетичний спектр.